THE ROYAL SOCIETY

Received 22 March 2004
Accepted 5 August 2004
Published online 23 November 2004

Empirically inspired simulated electro-mechanical model of the rat mystacial follicle–sinus complex

Ben Mitchinson[1], Kevin N. Gurney[1], Peter Redgrave[1], Chris Melhuish[2], Anthony G. Pipe[2], Martin Pearson[2], Ian Gilhespy[2] and Tony J. Prescott[1]*

[1]*Adaptive Behaviour Research Group, Department of Psychology, The University of Sheffield, Sheffield S10 2TP, UK*
[2]*Intelligent Autonomous Systems Laboratory, DuPont Building, University of the West of England, Coldharbour Lane, Frenchay, Bristol, BS16 1QY, UK*

In whiskered animals, activity is evoked in the primary sensory afferent cells (trigeminal nerve) by mechanical stimulation of the whiskers. In some cell populations this activity is correlated well with continuous stimulus parameters such as whisker deflection magnitude, but in others it is observed to represent events such as whisker-stimulator contact or detachment. The transduction process is mediated by the mechanics of the whisker shaft and follicle–sinus complex (FSC), and the mechanics and electro-chemistry of mechanoreceptors within the FSC. An understanding of this transduction process and the nature of the primary neural codes generated is crucial for understanding more central sensory processing in the thalamus and cortex. However, the details of the peripheral processing are currently poorly understood. To overcome this deficiency in our knowledge, we constructed a simulated electro-mechanical model of the whisker–FSC–mechanoreceptor system in the rat and tested it against a variety of data drawn from the literature. The agreement was good enough to suggest that the model captures many of the key features of the peripheral whisker system in the rat.

Keywords: whisker; follicle; model; mystacial; trigeminal; rat

1. INTRODUCTION

Many animals have a tactile sensory modality based upon an array of facial whiskers (Brecht *et al.* 1997). Because this modality is considered to be a good model of sensory systems in general, we expect to elucidate all sensory modalities through its investigation. Each whisker sits in a follicle in the mystacial pad of the face, where mechanoreceptors transduce whisker stimulation into neural signals. The follicle sits within a sinus, and together they form the follicle–sinus complex (FSC) (Rice *et al.* 1986). The signals enter the brain stem through trigeminal nerve cells (henceforth just 'cells'), and progress, primarily through the trigeminal complex and thalamus, to the barrel cortex (Welker *et al.* 1988). We are interested in computer modelling of this whisker–barrel pathway for two reasons. First, computational modelling is a powerful tool for understanding any complex biological system, of which the whisker–barrel system is certainly a prime example. Second, we are interested in developing better sensing technology using a biomimetic approach (Vincent 2003). In either enterprise, it is necessary to have a model of the initial stages of processing so that the input signals to subsequent stages are well grounded. Thus, we require a model of the whisker–FSC–mechanoreceptor system as a mechano-electric transducer. We chose to construct this model in software because this approach has a shorter development time than mechanical modelling.

Although the whisker–barrel system at and above the trigeminal complex contains multiple pathway loops (Welker *et al.* 1988; Kleinfeld *et al.* 1999), anatomical studies indicate no feedback connections to the FSC other than those associated with the musculature (Dörfl 1985; Rice *et al.* 1986). This suggests that the stimulus-to-trigeminal-nerve-activity transform is feedforward only. Electrophysiological studies show that the transform is nonlinear and state dependent; however, stimulus-strength to response-strength relationships are usually observed to be monotonic (e.g. Lichtenstein *et al.* 1990; Shoykhet *et al.* 2000). The transformation is a combination of mechanical processing amongst components of the whisker–FSC assembly and mechano–electric transduction within the FSC. Both mechanical information on the whisker–FSC assembly and electrophysiological information on mechanoreceptors is limited; the bulk of the available data consists of anatomical studies, and electrophysiological studies of the entire whisker–FSC–transduction system. Our procedure, then, is to postulate simple descriptions of mechanical and transductive components, guided by the anatomy, and attempt to reproduce aspects of these latter data.

2. EMPIRICAL BASES FOR THE MODEL

Around 50–200 cells innervate each FSC (Lee & Woolsey 1975). The classical study of their response involves head-fixing the animal, performing a controlled whisker deflection, and observing the characteristics of the evoked response train (*passive deflection study*) (Zucker & Welker 1969; Hahn 1971; Gottschaldt *et al.* 1973; Dykes 1975; Gottschaldt & Vahle-Hinz 1981; Gibson & Welker 1983*a*,*b*; Lichtenstein *et al.* 1990; Shoykhet *et al.* 2000). Baumann *et al.* (1996) applied a similar deflect and record technique to a whisker–FSC assembly isolated and fixed *in vitro*. Such studies have been performed with a variety of

*Author for correspondence (t.j.prescott@shef.ac.uk).

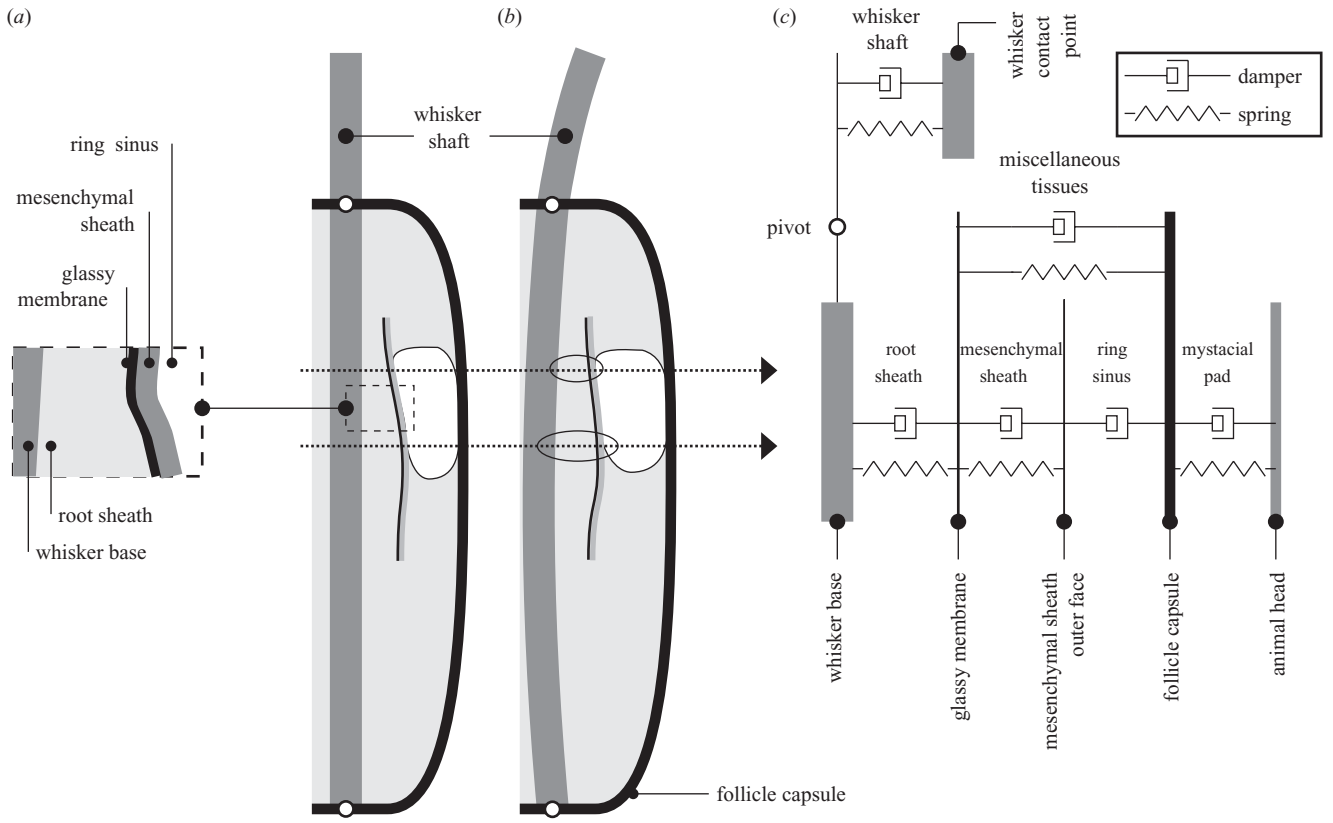

Figure 1. (*a*) Simplified FSC anatomy, (*b*) effect of deflection and (*c*) exploded FSC mechanical model. Ellipses indicate regions of coupling between modelled components and unmodelled components.

protocols, which makes collation of results difficult; however, on the following general points, most of the authors listed above agree.

Each cell responds to stimulation of one whisker only, and quiescent responses carry negligible information. Responses weaken as whisker deflections are maintained: the rate of adaptation to stimulus is used by almost all authors as the primary response classification; rapidly adapting (RA) and slowly adapting (SA) cells are distinguished. Cells begin responding at varying stimulus strengths. Most responses are directionally sensitive, this characteristic being most marked in SA cells. Increasing stimulus onset velocities elicit lower latency and higher spike counts from all cells; increasing stimulus deflection amplitudes elicit higher tonic firing rates from SA cells.

SA cells, therefore, appear to encode continuous stimuli, whereas RA cells encode changes in stimuli (e.g. onset and offset). Variation in response threshold (amplitude and velocity) and maximally effective angle (MEA) throughout the cell population leads to encoding of stimulus-strength (amplitude and velocity) and direction at the single-whisker level, complementing the cell level encoding. Furthermore, because each cell responds to one whisker only, stimulus location is encoded at the multi-whisker level.

Zucker & Welker (1969), as part of a wider study, artificially stimulated facial muscles to evoke a whisking-like movement and obstructed the whisker's path, while recording cell responses (*active deflection study*). This is a more naturalistic situation because the rat moves its whiskers during exploratory and investigative behaviour (Carvell & Simons 1990; Hartmann 2001). They observed that a response was evoked from *ca*. 50% of cells in the absence of, and 90% in the presence of, an obstacle and also observed repeatable temporal patterns in responses. Szwed *et al.* (2003) performed a similar study, replicated Zucker & Welker's results, and further analysed the response patterns. They sub-classified cells that responded only in the presence of an obstacle according to the feature to which they responded, thus: initial contact of whisker with obstacle (*contact*), detachment of whisker from obstacle (*detach*), both *contact*/*detach*, and entire contact period (*pressure*).

Finally, severing the afferent cells from the trigeminal complex does not affect their responses (Zucker & Welker 1969; Baumann *et al.* 1996), confirming the lack of feedback suggested by the anatomy.

3. MODEL DEVELOPMENT

(a) *Overview*

Some authors have suggested that the source of the most commonly observed touch response classes might be ascribed to mechanoreceptors identified at the level of the ring sinus (e.g. Gottschaldt *et al.* 1973). We therefore chose to model this level of the FSC only. We postulated that the free whisking responses observed by Szwed *et al.* (2003) spring from another level of the FSC, possibly the rete ridge collar, and did not attempt to model these. The FSC has a complex mechanical structure (Rice *et al.* 1986; Ebara *et al.* 2002) which we therefore assumed is able to make a substantial contribution to the overall behaviour. Indeed, it proved possible to obtain qualitative fits with the the main features of the data by simply interpreting the mechanical output of the FSC model as the mechanoreceptor signal. We thus incorporated a comparatively

simple model of the mechanoreceptor which was adequate to translate mechanical strain into spike trains and account for additional features of the data.

We made the assumption that each cell responds to stimulation of only one whisker, which is strongly supported by both physiological and anatomical studies. The RA/SA dichotomy was noted in all listed passive deflection studies, with the exception of the two part study by Gibson & Welker (1983*a*,*b*). We chose, therefore, to model two populations, responding to deflection and changes in deflection, although this is not a requirement of the model. Directional sensitivity is widely observed: we defined an MEA and a directional sensitivity between zero (not directionally sensitive) and unity (no response to deflection opposite MEA), and chose a circular form for the sensitivity function.

All aspects of the model were built under MATLAB (http://www.mathworks.com). All original software was written in-house, and the mechanical model was implemented using a fixed-step (10^{-6} s) discrete-time integration engine.

(b) *Whisker–follicle–sinus complex model*

Aspects of FSC anatomy (Dörfl 1985; Rice *et al.* 1986; Dehnhardt *et al.* 1999; Ebara *et al.* 2002) are distilled in figure 1*a*. In the rat, the follicle capsule is fairly rigid (Ebara *et al.* 2002), so we modelled it as a rigid component. We conglomerated inner and outer root sheaths such that the whisker base sits within a single elastic sheath (*root sheath*). Outside the root sheath is the glassy membrane, which we assumed is rigid. We modelled the mesenchymal sheath which sits outside the glassy membrane as another elastic sheath with its outer face free in the ring sinus. The root sheath, glassy membrane and mesenchymal sheath are also coupled to unmodelled parts of the FSC; we represented this coupling as 'miscellaneous tissues' between the glassy membrane and the follicle capsule. We ignored, for now, the ringwulst, despite the intriguing suggestion in (Rice *et al.* 1986) that it may form part of an acceleration detector. As a result, we did not distinguish between the lanceolate and club-like endings (Ebara *et al.* 2002) in the mesenchymal sheath.

Figure 1*b* shows our concept of the effect of deflection; the base of the whisker moves in the opposite direction to the tip. One can intuit from the diagram that there is not a linear relationship between external whisker deflection and internal deformation; however, when this relationship is analysed (analysis not shown), it is seen to be extremely close to linear, so we made this simplification.

Because the follicle is more or less symmetric about its longitudinal axis (at least at the ring sinus level), we reduced it to a one-dimensional radial representation. We modelled the components as a linear discrete-time mass/spring/damper system, a schematic of which is given in figure 1*c*. The FSC moving parts are the whisker base, glassy membrane, mesenchymal sheath outer face and follicle capsule. The root and mesenchymal sheaths were modelled as damped springs, and the ring sinus as a pure damper. Because the whisker base is moved indirectly by the whisker shaft, we needed a model of the shaft to complete the route from stimulus to mechanoreceptor. We chose a damped spring for the whisker shaft, and added the whisker contact point as an extra moving part. The mechanical advantage given by the whisker is modelled as a lever between the whisker base and contact point, pivoting at the skin. Finally, we acknowledge that the FSC itself is not fixed in the head, and couple it to an immovable base (the animal head) through a damped spring.

Table 1. Mechanical model parameters: captions indicate how chosen. ~ and † indicate categories of robustness, detailed in § 4.
WB, whisker base; GM, glassy membrane; MSO, mesenchymal sheath outer face; FC, follicle capsule; RS, root sheath; MS, mesenchymal sheath; MT, miscellaneous tissues; WS, whisker shaft; MP, mystacial pad; SI, ring sinus; WC, whisker contact point.)

parameter	value	robustness
estimated from anatomy		
m_{WB}	20 µg	~
m_{GM}	25 µg	†
m_{MSO}	5 µg	~
m_{FC}	500 µg	~
k_{RS}	20 kNm^{-1}	†
k_{MS}	100 kNm^{-1}	~
critical damping		
d_{RS}	$2\sqrt{m_{GM}k_{RS}}$ Ns m^{-1}	~
d_{MS}	$2\sqrt{m_{MSo}k_{MS}}$ Ns m^{-1}	~
d_{MT}	$2\sqrt{m_{GM}k_{MT}}$ Ns m^{-1}	†
d_{WS}	$2\sqrt{m_{WC}k_{WS}}$ Ns m^{-1}	~
d_{MP}	$2\sqrt{m_{FC}k_{MP}}$ Ns m^{-1}	~
d_{SI}	$2\sqrt{m_{GM}k_{RS}}$ Ns m^{-1}	†
chosen to allow only limited follicle movement		
k_{MP}	100 kNm^{-1}	~
tuned to observations		
m_{WC}	0.5 µg	†
k_{MT}	50 Nm^{-1}	†
k_{WS}	100 kNm^{-1}	~
l	$-0.27/\sqrt{h}$	—

We denote mass, spring constants and damper constants of a component, Q, as m_Q, k_Q and d_Q, respectively, and its deflection from rest in the plane of the skin as the two-dimensional vector $\boldsymbol{P}_{Q,n}$ with n the sample number. The abbreviations for the components can be found in the caption of table 1. We estimated the masses of the components based on their dimensions and density, except for m_{WC}, because the contact point is not defined as an object with dimension. We estimated some spring constants based on their spatial dimensions and Young's modulus (E). We took dimensions from Rice *et al.* (1986) and chose a density of 2 mg mm^{-3} for all components. Measurements of Young's modulus of rat skin vary greatly, but 10 MPa is an order of magnitude estimate (Ozyazgan *et al.* 2002); we therefore chose 10 MPa as an order of magnitude estimate for E of the follicle components. We chose all damping constants to critically damp their most closely associated mass, as measured whisker–FSC dynamic behaviours are in this region (Hartmann *et al.* 2003). k_{MP} was chosen to allow only limited follicle movement when the whisker is deflected, and the remaining constants were tuned to optimize the fit to observed data. We denote the advantage of the lever as l, and chose a formula for this parameter by rough tuning to observed data, with h the distance between the contact point and the skin surface. The parameters are summarized in table 1.

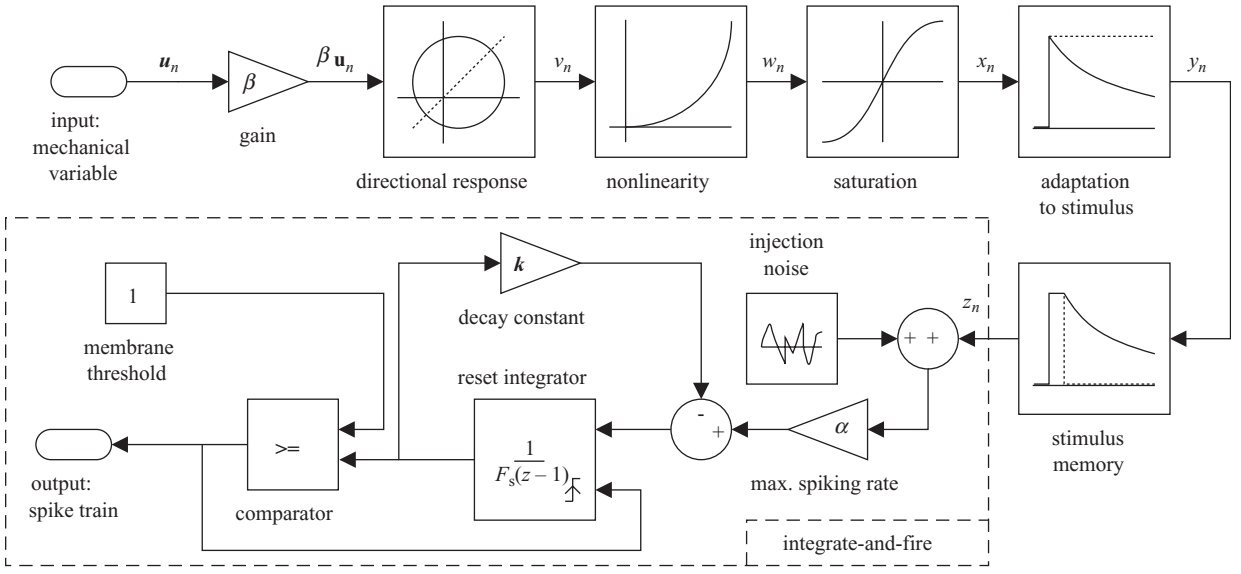

Figure 2. Mechanoreceptor model: the input (mechanical strain, $\boldsymbol{u}_n$) is transformed, in turn, by processing units representing directional response, nonlinearity, saturation, adaptation to stimulus and stimulus memory; the resulting signal (z_n) drives a conventional integrate-and-fire membrane model. Details of these components can be found in the text.

(c) *Mechanoreceptor model*

Mechanoreceptors are found on either side of the glassy membrane at the level of the ring sinus, Merkel endings inside, and lanceolate/club-like endings outside (Rice *et al.* 1986; Ebara *et al.* 2002; Maklad *et al.* 2004). Although we wish to model a variety of signal processing in the mechanoreceptors, we decided not to try and develop a realistic biophysical model that could provide a biological grounding for such processing, owing to time limitations. Rather, we adopted an approach in which each required function of the mechanoreceptor was modelled phenomenologically by a discrete processing stage. However, we would anticipate that some of these functions may be supported by the membrane dynamics of the mechanoreceptors themselves.

We divided our model mechanoreceptors into two classes that support SA and RA responses (same model structure, different parameters). We tentatively identified the two classes with the Merkel and lanceolate endings, respectively, a suggestion that has been put forward previously (Waite & Tracey 1995; Ebara *et al.* 2002), and thus located them inside and outside the glassy membrane, respectively. For mechanoelectric transduction to occur in these cells, they must respond to deformation: the input to a cell model, then, is the discrete-time strain in the spring representing the layer in which it lies. Strain is defined as change in length over unstressed length, so we write the strains in the two layers as $\boldsymbol{u}_{\mathrm{RS},n} = (\boldsymbol{p}_{\mathrm{GM},n} - \boldsymbol{p}_{\mathrm{WB},n})/t_{\mathrm{RS}}$ and $\boldsymbol{u}_{\mathrm{MS},n} = (\boldsymbol{p}_{\mathrm{MSO},n} - \boldsymbol{p}_{\mathrm{GM},n})/t_{\mathrm{MS}}$, with the layer thicknesses $t_{\mathrm{RS}} = 80\,\mu\mathrm{m}$ and $t_{\mathrm{MS}} = 20\,\mu\mathrm{m}$ taken from the anatomy (Rice *et al.* 1986). Increasing stimulus velocities and amplitudes thus naturally lead to higher firing rates. The cell model is illustrated schematically in figure 2; the labels in that figure correspond to the variables used below. For notational convenience, we drop the component subscripts from $\boldsymbol{u}_{\mathrm{RS},n}$ and $\boldsymbol{u}_{\mathrm{MS},n}$ and represent either as $\boldsymbol{u}_n$.

The gain, β, fixes the cell's response range. The direction-dependent gain (which simulates directional sensitivity) is given by

$$v_n = |\beta \boldsymbol{u}_n| \frac{\sqrt{b^2 - 4c} - b}{2}, \tag{3.1}$$

$$b = -\zeta \cos(\arctan(u_{n,2}/u_{n,1}) - \theta), \tag{3.2}$$

$$c = (\zeta/2)^2 - (1 - \zeta/2)^2, \tag{3.3}$$

where $\boldsymbol{u}_n = [u_{n,1}, u_{n,2}]$. This defines a circular function with unity gain at the MEA ($\theta \in [0,2\pi)$), and a gain of $1 - \zeta$ opposite the MEA, $\zeta \in [0,1]$. The nonlinearity $w_n = v_n^{\gamma}$ was used to modify the response profile of the cell to fit observations. A saturation unit $x_n = \tanh(w_n)$ limits the cell firing rate. Adaptation to stimulus was modelled as

$$y_n = x_n - q_n, \tag{3.4}$$

$$q_n = (1 - \lambda_{\mathrm{A}})x_n + \lambda_{\mathrm{A}} q_{n-1}, \tag{3.5}$$

$$\lambda_{\mathrm{A}} = \exp(-1/(\tau_{\mathrm{A}} F_s)), \tag{3.6}$$

with $1/F_s$ the sample period of integration, τ_{A} the adaptation time constant, and q_n an internal state. y_n, thus, closely follows features in x_n with duration much less than τ_{A}, but responds decreasingly to features with longer durations. Stimulus memory was modelled as

$$z_n = \begin{cases} y_n, & y_n > \lambda_{\mathrm{M}} z_{n-1} \\ \lambda_{\mathrm{M}} z_{n-1}, & \text{otherwise} \end{cases}, \tag{3.7}$$

$$\lambda_{\mathrm{M}} = \exp(-1/(\tau_{\mathrm{M}} F_s)). \tag{3.8}$$

The resulting response-strength, z_n, forms the input of an integrate-and-fire neuronal cell model (Eliasmith & Anderson 2003) which generates the spike train. This consists of a leaky integrator with membrane decay constant $k = 1 - \exp(-1/(\tau_{\mathrm{D}} F_s))$ that resets when its output reaches a fixed unity threshold (τ_{D} is the membrane time constant). Gaussian white noise $N(\mu,\sigma^2)$ is added to the injection current, before scaling by the desired maximum firing rate, α. Finally, all spikes are delayed by a

fixed amount τ_L (not shown) to simulate the transmission latency in components including the nerve cell.

For the membrane, we chose a typical value for τ_D (Koch 1999), and set α to allow for all observations in all the studies considered. A small amount of injection noise was chosen to linearize the membrane while keeping the quiescent firing rate below about one spike per second; this is expedient for tuning and has little effect on overall behaviour. Initial gains (β) were chosen such that typical stimuli gave approximately unity-scaled responses; later they were tuned against observed data. All remaining parameters were chosen to match observations, and are summarized in table 2*a*. This set of parameters defines 'typical' SA and RA cells. To construct a follicle population of cells, we can allow some variation in some or all of these. We chose to allow only β and τ_A to vary, because both of these are seen to vary in many of the cited studies. The variation we chose was based on observation, and is given in table 2*b*.

(**d**) *Using the model*

To simulate a study, we use the same number of cells of each class (SA/RA) as were observed, distributing their MEAs uniformly across the range. We then drive the model in one of two modes: to simulate a passive deflection study, we drive m_{WC} (whisker contact point) and allow the remaining components to move freely, except the animal head which remains fixed; to simulate an active deflection study, we drive m_{FC} (follicle capsule), constrain m_{WC}, and allow the remaining components to move freely. The outputs from the mechanical model are the strains in k_{RS} (root sheath) and k_{MS} (mesenchymal sheath). We approximate the driving stimulus described in the study, to generate follicle strain profiles. Finally, we simulate each of the cells in turn to generate 'recorded' responses.

4. RESULTS

(**a**) *Strain profiles*

Figure 3 shows typical strain profiles evoked by passive and active model stimulation. The strains in the root and mesenchymal sheaths are given to a first approximation by $a\dot{\boldsymbol{x}}$ and $b\boldsymbol{x}+c\dot{\boldsymbol{x}}$, where $\boldsymbol{x}=\boldsymbol{x}_{WB}-\boldsymbol{x}_{FC}$. Thus, the FSC mechanically takes a derivative of the position of the whisker base relative to the follicle capsule. Under passive deflection conditions with a stimulator contact point near the skin, $\boldsymbol{x}_{WB}$ is approximately proportional to $\boldsymbol{x}_{WC}$, and the deflection of the whisker contact point is encoded in a straightforward manner, but other conditions lead to a more complex response.

(**b**) *Robustness*

Because we had limited information to help us choose the parameters of the mechanical model, we were interested in the robustness of the model to their variation. We tested this by generating the profiles of figure 3 while varying parameter values. The effects are recorded in the final column of table 1. Varying those marked '~' by an order of magnitude in either direction had an insubstantial effect on the strain profiles (other than, in some cases, a scaling). When varying those marked '†' by an order of magnitude in either direction, any resulting changes to the profiles could be reversed by varying one or more of the other parameters in this set by no more than an order of magnitude. This latter set of six parameters dictate the behaviour of the model, giving three basic degrees of freedom (*a*, *b* and *c* from the above equations) and a fourth, which controls the transient behaviour of the model. Of these six parameters, four are fixed in the development (see table 1), so only two must be tuned to fit observations.

Table 2. (*a*) Mechanoreceptor model parameters for a typical cell and (*b*) variations introduced when modelling population. *R*(.) is the Rayleigh distribution (*R* (1) inset).

parameter	SA	RA
(*a*)		
τ_D	10 ms	10 ms
α	1000	2000
μ	0.05	0.03
σ	0.1	0.1
β	18.8	61.5
ς	1	0.6
γ	1	2
τ_A	1 s	5 ms
τ_M	5 ms	5 ms
τ_L	3 ms	3 ms
(*b*)		
$\beta\times$	$0.25+\mathrm{R}(0.75)$	$0.5+\mathrm{R}(0.5)$
$\tau_A\times$	$0.5+\mathrm{R}(0.5)$	$0.5+\mathrm{R}(0.5)$

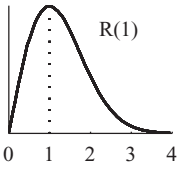

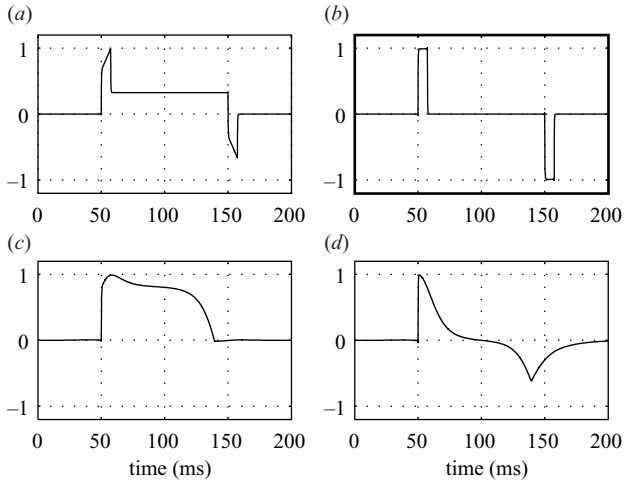

Figure 3. Typical (normalized) strain profiles evoked in root sheath (*a*,*c*) and mesenchymal sheath (*b*,*d*) during simulated passive (*a*,*b*) and active (*c*,*d*) deflection studies. Stimulator is 5 mm (*a*,*b*) or obstacle is 40 mm (*c*,*d*) from skin.

(**c**) *Validation*

We adjusted the free parameters of the model to attempt to reasonably fit most of the results reported in the response studies listed in § 2. Because of space limitations we cannot present all comparisons, so we choose to present comparisons only with two passive studies (Lichtenstein *et al.* 1990; Shoykhet *et al.* 2000) and the active study (Szwed *et al.* 2003).

Lichtenstein *et al.* (1990) applied a single trapezoidal stimulus in eight directions while recording from a total of 123 cells (92 were classified SA, 31 RA). In figure 4 we reproduce figure 1 from that study, which shows peristimulus time histograms (PSTHs) from two typical cells. For comparison, we also present PSTHs generated by the model during an equivalent simulation. Response

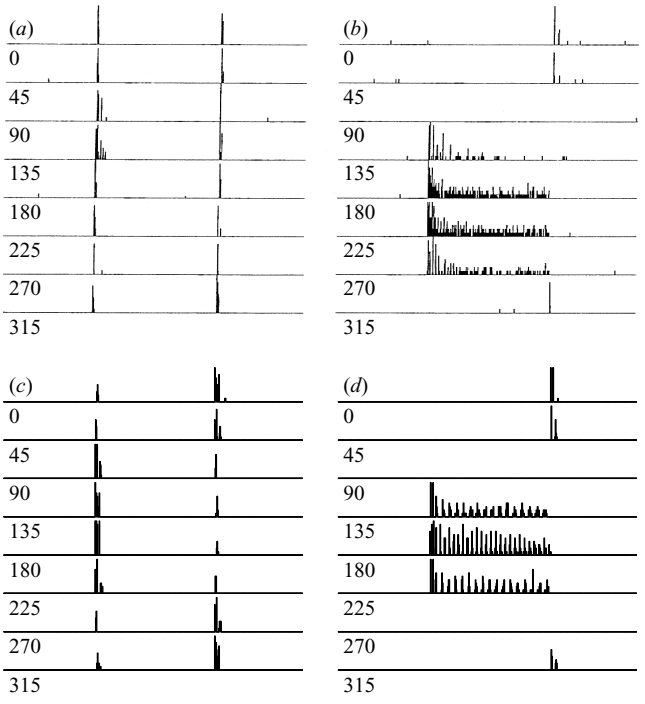

Figure 4. Peri-stimulus time histograms (PSTHs) from (*a*) RA and (*b*) SA cells during trapezoidal deflection in eight different directions, reprinted (some components regenerated for clarity) from Lichtenstein *et al.* (1990) with permission from Taylor & Francis Ltd (http://www.tandf.co.uk/journals). Equivalent PSTHs from model (*c*) RA and (*d*) SA cells during simulated protocol.

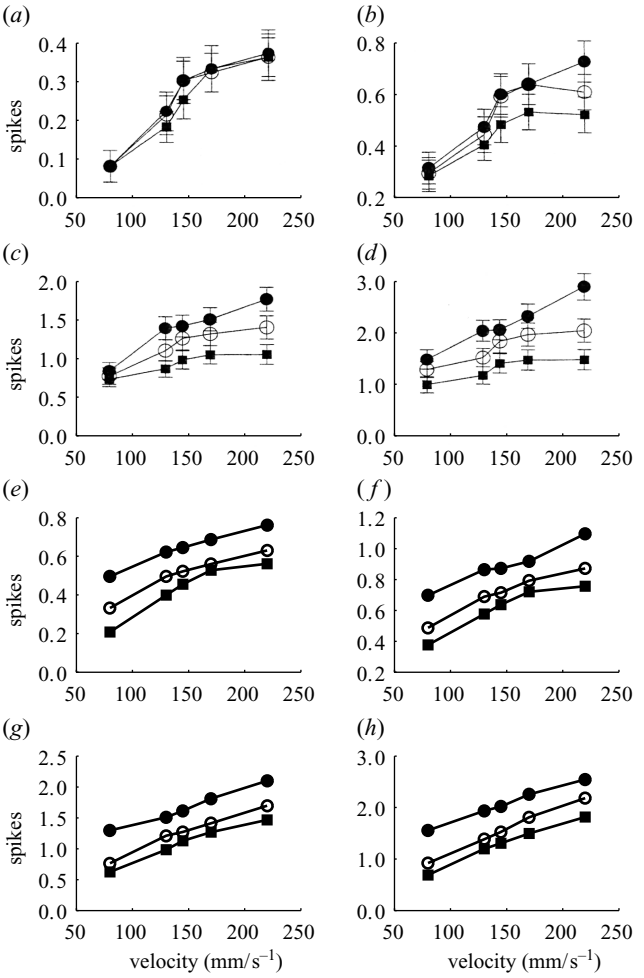

Figure 5. Average number of spikes discharged by SA cells during various time epochs after population response onset: (*a*) 1.2 ms; (*b*) 2.0 ms; (*c*) 5.0 ms; and (*d*) 8.0 ms. Reprinted (some components regenerated for clarity) from Shoykhet *et al.* (2000) with permission from Taylor & Francis Ltd. Equivalent output from model SA cells during simulated protocol: (*e*) 1.2 ms; (*f*) 2.0 ms; (*g*) 5.0 ms; and (*h*) 8.0 ms . Closed circles, 650 μm; open circles, 390 μm; closed squares, 225 μm (deflection amplitude).

envelopes are in good agreement throughout, however the model SA cell has a more regular firing pattern than the real one.

Shoykhet *et al.* (2000) applied a trapezoidal stimulus at the MEA only while recording from 81 cells (60 SA, 21 RA), using five different velocities and three different amplitudes. In figure 5 we reproduce figure 5 from that study, which shows average spike counts in the SA cells during four different epochs after population response onset. We present the corresponding result from the model underneath. The only substantial disagreement is that the model cells encode amplitude earlier in the response than the real cells.

Szwed *et al.* (2003) induced artificial whisking at 5 Hz. The stimulus profile was dictated by the response of the muscles, and can be seen in their original work. They placed an obstacle in the path of the whisker at 80–90% of the whisker length, and recorded from 30 cells that responded only in the obstacle's presence (11 SA, 19 RA). We approximated their whisking profile by driving the follicle with the function

$$\boldsymbol{P}_{\mathrm{FC}} = [-0.15 \tanh(2 \sin(10\pi t)), 0], \tag{4.1}$$

(which is a sine function with flattened peaks) while constraining $\boldsymbol{P}_{\mathrm{WC}}$ to be less than 0 (modelling an obstacle in the whisker's path), and used a contact point 40 mm from the skin. RA cells that had a spike count an order of magnitude greater in response to either contact or detach were classed accordingly. SA cells were all classed as pressure cells. In figure 6 we reproduce figure 2*a* from their study, which shows PSTHs from contact, detach, and pressure cells, averaged over all trials. For comparison, we present the corresponding result from the model underneath. Qualitatively, the response of the model agrees well with observation: in particular, there are obvious contact, detach, and pressure responses, as seen in the real cells. The cycle is somewhat shorter in the model, indicating that our driving profile is not a match for that produced by the muscles, and the model cells respond much more strongly to the stimulus.

5. DISCUSSION

Regarding the mechanics, the early encoding of amplitude by the model SA cells relative to real SA cells (figure 5) is a real discrepancy, but we are confident that it can be corrected by adjusting the model. It is possible to reduce the response of the model in the active deflection simulation illustrated in figure 6, but the adjustment leads to a corresponding decrease in response in the other studies. We believe that, because the link between the two types of

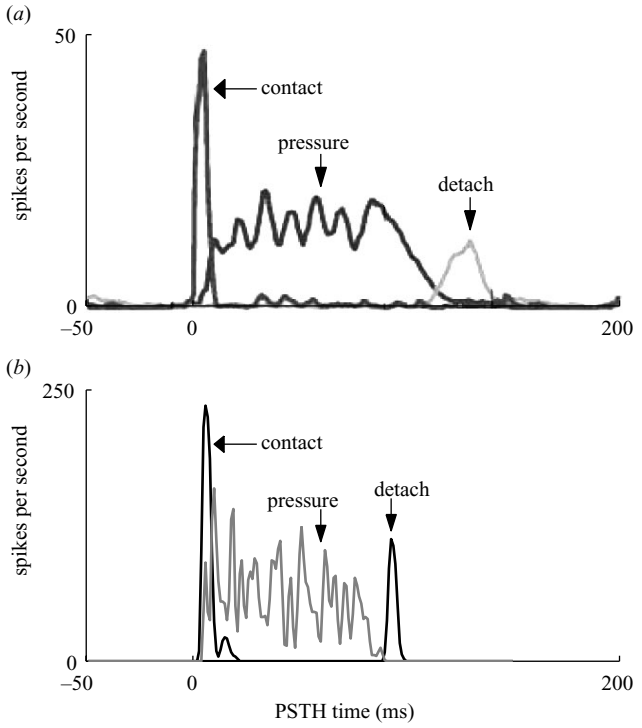

Figure 6. (*a*) PSTHs averaged over contact, detach and pressure cells during whisking against an obstacle, reprinted (some components regenerated for clarity) from Szwed *et al.* (2003) with permission from Elsevier. (*b*) Equivalent output from model cells during simulated protocol.

studies is primarily provided by the whisker shaft model, this component needs to be refined. In the model, there is a strong correlation between MEA and the sub-class of cell (contact, detach) observed in the active deflection simulation, which was not found by (Szwed *et al.* 2003). We do not believe that this undermines the model, but the matter needs further investigation.

Szwed *et al.* (2003) also found responses that were present even when a whisker obstacle was not present; we suggest that these, fundamentally different, response types, have their origin in another region of the FSC. In particular, we suggest that the upper regions (probably rete ridge collar though also possibly outer conical body) are more suited to generating these types of response because they interact with a stationary reference point (the mystacial pad); the possibility that these responses are generated inertially cannot be excluded, however.

Regarding the mechanoreceptors, both irregularly and regularly firing SA responses have been observed in the biology (named, respectively, SAI and SAII responses (Gottschaldt *et al.* 1973)), whereas the simple mechanoreceptor model used here leads only to the regular firing illustrated in figure 4. The phenomenon of 'phase-locking' (synchronizing of response spikes to phase of vibratory stimuli) has been reported in several works, but we do not attempt to reproduce it here. More accurate reproduction of spike trains on small time-scales might be achieved by incorporating the more detailed Hodgkin–Huxley-based mechanoreceptor model by Bell & Holmes (1992).

It is difficult to proceed further with a bottom-up development of this model without additional mechanical analysis of the components of the whisker–FSC assembly. Further top-down development of this model would be eased by targeted engineering analysis of the whisker–FSC as a transducer.

In summary, we have presented what is, to our knowledge, the first quantitative biologically plausible model of the rat whisker FSC. The model can account for a variety of results from deflection studies including: directionality, transient and sustained responses, encoding of stimulus amplitude and velocity in firing rate, and furthermore links results from passive and active deflection studies. Also, we have shown that some of the main features of the data may be explained as a result of 'computations' performed mechanically in the follicle complex itself. Finally, the model is parametrically robust with just four essential degrees of freedom. We therefore anticipate that accounts in more refined models will not substantially differ from that given here.

The authors acknowledge technical discussions with Marcin Szwed, Ehud Ahissar and Satomi Ebara, and the comments of the anonymous reviewers. This work was funded by EPSRC Research grant no. GR/S19639/01.

REFERENCES

Baumann, K., Chan, E., Halata, Z., Senok, S. & Yung, W. 1996 An isolated rat vibrissal preparation with stable responses of slowly adapting echanoreceptors. *Neurosci. Lett.* **213**, 1–4.

Bell, J. & Holmes, M. 1992 Model of the dynamics of receptor potential in a mechanoreceptor. *Math. Biosci.* **110**, 139–174.

Brecht, M., Preilowski, B. & Merzenich, M. 1997 Functional architecture of the mystacial vibrissae. *Behav. Brain Res.* **84**, 81–97.

Carvell, G. & Simons, D. 1990 Biometric analyses of vibrissal tactile discrimination in the rat. *J. Neurosci.* **10**, 2638–2648.

Dehnhardt, G., Hyvärinen, H., Palviainen, A. & Klauer, G. 1999 Structure and innervation of the vibrissal follicle-sinus complex in the Australian water rat, *Hydromys chrysogaster*. *J. Comp. Neurol.* **411**, 550–562.

Dörfl, J. 1985 The innervation of the mystacial region of the white mouse. A topographical study. *J. Anat.* **142**, 173–184.

Dykes, R. 1975 Afferent fibers from mystacial vibrissae of cats and seals. *J. Neurophysiol.* **38**, 650–662.

Ebara, S., Kumamoto, K., Matsuura, T., Mazurkiewicz, J. & Rice, F. 2002 Similarities and differences in the innervation of mystacial vibrissal follicle-sinus complexes in the rat and cat: a confocal microscopic study. *J. Comp. Neurol.* **449**, 103–119.

Eliasmith, C. & Anderson, C. 2003 *Neural engineering*. Cambridge, MA: MIT Press.

Gibson, J. & Welker, W. 1983*a* Quantitative studies of stimulus coding in first-order vibrissa afferents of rats. 1. Receptive field properties and threshold distributions. *Somatosens. Res.* **1**, 51–67.

Gibson, J. & Welker, W. 1983*b* Quantitative studies of stimulus coding in first-order vibrissa afferents of rats. 2. Adaptation and coding of stimulus parameters. *Somatosens. Res.* **1**, 95–117.

Gottschaldt, K. & Vahle-Hinz, C. 1981 Merkel cell receptors: structure and transducer function. *Science* **214**, 183–186.

Gottschaldt, K., Iggo, A. & Young, D. 1973 Functional characteristics of mechanoreceptors in sinus hair follicles of the cat. *J. Physiol.* **235**, 287–315.

Hahn, J. 1971 Stimulus–response relationships in first-order sensory fibres from cat vibrissae. *J. Physiol.* **213**, 215–226.

Hartmann, M. 2001 Active sensing capabilities of the rat whisker system. *Autonomous Robots* **11**, 249–254.

Hartmann, M., Johnson, N., Towal, R. & Assad, C. 2003 Mechanical characteristics of rat vibrissae: resonant frequencies and damping in isolated whiskers and in the awake behaving animal. *J. Neurosci.* **23**, 6510–6519.

Kleinfeld, D., Berg, R. & O'Connor, S. 1999 Anatomical loops and their electrical dynamics in relation to whisking by rat. *Somatosens. Motor Res.* **16**, 69–88.

Koch, C. 1999 *Biophysics of computation*. Oxford University Press.

Lee, K. & Woolsey, T. 1975 A proportional relationship between peripheral innervation density and cortical neuron number in the somatosensory system of the mouse. *Brain Res.* **99**, 349–353.

Lichtenstein, S., Carvell, G. & Simons, D. 1990 Responses of rat trigeminal ganglion neurons to movements of vibrissae in different directions. *Somatosens. Motor Res.* **7**, 47–65.

Maklad, A., Fritzsch, B. & Hansen, L. 2004 Innervation of the maxillary vibrissae in mice as revealed by anterograde and retrograde tract tracing. *Cell Tissue Res.* **315**, 167–180.

Ozyazgan, I., Liman, N., Dursun, N. & Günes, I. 2002 The effects of ovariectomy on the mechanical properties of skin in rats. *Maturitas* **43**, 65–74.

Rice, F., Mance, A. & Munger, B. 1986 A comparative light microscopic analysis of the sensory innervation of the mystacial pad. I. Innervation of vibrissal follicle-sinus complexes. *J. Comp. Neurol.* **252**, 154–174.

Shoykhet, M., Doherty, D. & Simons, D. 2000 Coding of deflection velocity and amplitude by whisker primary afferent neurons: implications for higher level processing. *Somatosens. Motor Res.* **17**, 171–180.

Szwed, M., Bagdasarian, K. & Ahissar, E. 2003 Encoding of vibrissal active touch. *Neuron* **40**, 621–630.

Vincent, J. F. V. 2003 Biomimetic modelling. *Phil. Trans. R. Soc. Lond.* B **358**, 1597–1603. (doi:10.1098/rstb.2003.1349)

Waite, P. & Tracey, D. 1995 Trigeminal sensory system. In *The rat nervous system* (ed. G. Paxinos), pp. 705–724. San Diego, CA: Academic.

Welker, E., Hoogland, P. & Van der Loos, H. 1988 Organization of feedback and feedforward projections of the barrel cortex: a PHA-L study in the mouse. *Exp. Brain Res.* **73**, 411–435.

Zucker, E. & Welker, W. 1969 Coding of somatic sensory input by vibrissae neurons in the rat's trigeminal ganglion. *Brain Res.* **12**, 138–156.

As this paper exceeds the maximum length normally permitted, the authors have agreed to contribute to production costs.